In-situ pH Measurement of Water Droplets Using Flash-Freeze SERS

Qishen Huang[1,2], *Peter J. Vikesland*[1,2*]

[1] Department of Civil and Environmental Engineering, Virginia Tech, Blacksburg, Virginia;

[2] Virginia Tech Institute of Critical Technology and Applied Science (ICTAS) Sustainable Nanotechnology Center, Blacksburg, Virginia;

Keywords: Environmental droplet, pH, flash-freeze SERS.

*Corresponding Author e-mail: pvikes@vt.edu

Abstract

Characterization of single droplet pH is required to better understand differences in droplet and bulk water chemistries and the variability of individual atmospheric droplets. In this study, we demonstrate the use of flash-freeze SERS as a means to characterize the pH of micron-size droplets generated from mixtures of low solute concentration environmental water samples and a pH nanoprobe. These samples included stream waters, rain, and snowmelt from areas surrounding Blacksburg, Virginia. Compared to room-temperature SERS, flash-freeze SERS preserves the initial droplet properties and minimizes water loss due to localized heat generation in the vicinity of SERS hot-spots. Moreover, the flash-freeze SERS approach provides greater sensitivity relative to pH paper for low solute concentration droplets. We observed that pH values measured by flash-freeze SERS were generally comparable with those obtained at room temperature, but did not result in heating induced droplet destabilization. Using flash-freeze SERS, we observed that droplet and bulk pH were comparable for most environmental samples. One rainwater sample showed a higher droplet pH compared to its bulk sample. Based upon ICP-MS results, the ionic composition of this rainwater was significantly different from the other collected samples, thus suggesting the effect of droplet composition on droplet pH. Our results demonstrate the application of the flash-freeze SERS method to preserve environmental droplet properties and to measure pH of low solute concentration droplets.

Keywords: Aerosol droplets; Raman; SERS; pH; flash-freeze

Synopsis: We illustrate the utility of flash-freeze SERS for characterization of the pH of environmental water samples.

TOC art

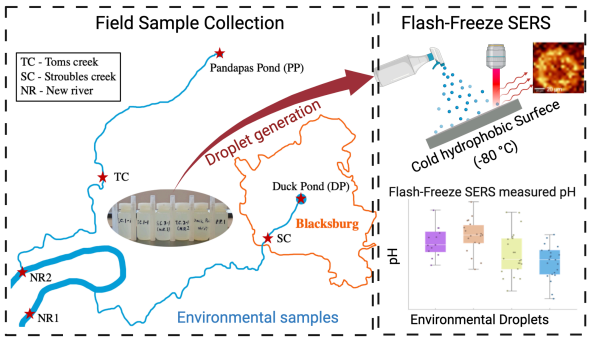

Introduction

Aerosols and aqueous droplets are ubiquitous in the atmosphere. Among the physiochemical properties that describe atmospheric droplets, pH is a crucial factor affecting the thermodynamics of gas-liquid partitioning at the air-water interface and atmospheric chemical kinetics (e.g., aerosol formation and transportation).[1–3] Accurate characterization of atmospheric droplet pH is needed to improve our understanding and prediction of the effect of atmospheric droplets on climate, human health, and ecosystems.[3,4]

Atmospheric droplet pH exhibits extensive temporal and spatial variations that reflect changes in droplet composition as droplets evolve in the atmosphere. The pH of sea spray aerosols is typically around 7-8 upon generation, but rapidly decreases due to the uptake of acidic gases such as SO_2 and HNO_3.[5–8] In addition, relative humidity (RH) affects the water content of atmospheric droplets. Processes such as deliquescence (transition from solid particles into aqueous droplets through water uptake) and efflorescence (transition from aqueous droplets to solid particles via evaporation) are RH driven.[9,10] As the water content of a droplet varies, solute concentrations change thus affecting the equilibrium state of the droplets.[11,12] Due to the close correlation between

droplet composition and pH there is need for the development of droplet pH characterization methods that minimally affect droplet composition.

Raman spectroscopy provides rich chemical fingerprints for many dissolved analytes.[13,14] Surface-enhanced Raman spectroscopy (SERS), enabled by the local plasmon resonance at a noble metal interface (e.g., gold nanoparticles (AuNPs)), can enhance Raman signal intensities by up to 10^8.[15] SERS-enabled pH characterization methods have been applied in various systems.[16–20] Our group has pioneered the use of pH nanoprobe based SERS methods to characterize single droplet pH.[21–23] To study droplets generated from environmental samples characterized by low solute concentrations, we developed a flash-freeze SERS method to prevent droplet destabilization that may arise due to localized heat generation at SERS hot spots.[24–26]

Kucinski et al observed liquid-liquid phase separation of micron and sub-micron aerosols using flash-freeze flow tube and cryogenic transmission electron microscopy.[27] Inspired by this flash-freeze method and the use of vitrification within the biosciences,[28,29] we flash-froze droplets generated from environmental samples and characterized droplet pH via SERS. The flash-freeze process hinders ice nucleation and crystal growth and thus preserves the component distribution within droplets following aerosolization.[27,30,31] Importantly, low temperatures can effectively dissipate heat generated during SERS measurements. Herein, we present proof of concept results of the flash-freeze SERS method for environmental droplet pH characterization and show its protentional for onsite application and 2D imaging of environmental micrometer scale droplets.

Material and Methods

Environmental water samples

Stream and pond water samples were collected from six different locations within the New River Valley area of Virginia. Locations and sample abbreviations are marked in Figure 1a (SC-

Stroubles Creek, TC–Toms Creek, NR–New River, DP–Duck Pond, PP–Pandapas Pond). Rain samples were collected in December 2017 (R1217), August 2018 (R0818), and March 2021 (R0321). Snow samples were collected in March 2018 (S0318), December 2018 (S1218), and February 2021 (S0221) and were stored at -80°C immediately after collection. The snow samples were melted at room temperature prior to measurement. Acidic samples were prepared by adding 1-5 mM H_2SO_4 to the environmental samples. All bulk sample pH values were recorded using a commercial pH meter (Orion versa star pro, Thermo Scientific). The ionic composition of field samples were characterized via Inductively Coupled Plasma-Mass Spectrometry (ICP-MS, Thermo Scientific Thermo Electron X Series, Table S1).

Synthesis of pH nanoprobes and AuNS

SERS pH nanoprobes were synthesized via our previously reported approach.[21,23,32] The synthesis of gold nanostars (AuNS) followed the method of Yuan et al.[33] Detailed synthesis procedures, nanoparticle characterization, and the pH response of the pH nanoprobe are presented in the Supporting Information (SI).

Generation and Collection of Aerosol Droplets

Aerosol droplets were generated from the mixture of environmental samples and pH nanoprobe/AuNS suspensions using commercial spray bottles (10mL). The mixture contained 5% v/v nanoprobe which showed negligible effect on environmental sample pH (Table S2). Droplets were collected on a superhydrophobic filter,[22,23] with 4-6 times of spray. The high relative humidity (RH≈95%) room temperature SERS measurements follow our previously reported procedure.[22,23] The flash-freeze SERS measurements were conducted using a pre-cooled Linkam THM600 thermostage (-80°C). Droplet flash-freezing is described in detail in the Supporting Information

(SI). The collected droplet size ranged from 30-140 μm with an average of 80.3±21.8 μm. (Figure S2)

SERS measurements

SERS images of single droplets were collected using a confocal Raman microscope (WITec Alpha 500R, 50× objective lens, 785nm laser). The laser power was 2-10mW and the integration time was 0.2s for all measurements. SERS images of droplets at room temperature consisted of 10×10 pixels which represents an area covering an entire droplet. SERS images of flash-frozen droplets used 20×20 pixels over the droplet area for better spatial resolution. Bulk environmental sample pH values were measured in triplicate and each measurement was averaged from 20×20 spectra over a 100×100 μm^2 area.

pH characterization with pH paper.

We also characterized solution pH using pH paper (Hydrion, 1.0-12.0). The pH values of high concentration solutions were adjusted using 31.6mM HCl and 100 mM NaOH, while the pH of low concentration solutions were adjusted using 1mM HCl and 10mM NaOH. The pH of bulk and spray samples of all environmental samples were characterized using pH paper.

Results and Discussion

The limitations of room-temperature SERS for droplet pH quantification.

We previously observed changes in droplet pH measurements under low salt concentration (< 60mM) conditions that were attributed to water loss and efflorescence resulting from the heat generated during a room-temperature SERS measurement.[23] Such a heat effect limits the application of SERS for droplet characterization since atmospheric droplets often contain low solute concentrations. To examine the effect of heat on environmental droplets, we initially characterized droplet pH at room temperature and 95% RH following our previously reported

SERS method.[22,23] As shown in Figure 1b, following a room temperature SERS scan at 95% RH, the droplet diameter decreased to ~20μm from ~50μm due to water loss. Simultaneously, the brightness of a majority of the droplets (>70%) changed due to the change in light-scattering that results from droplet efflorescence.[34,35] Using XY-SERS scanning, we obtained SERS images that reveal the distribution of pH nanoprobes in droplets according to the characteristic peak at 1080 cm^{-1} (i.e., the ring-breathing mode of benzene[21]). SERS maps of pH nanoprobes collected from effloresced (i.e., optically darkened) droplets exhibit localized intensities that denote heterogeneous distributions that arise due to ice crystal formation (Figure 1b, Figure S3). We differentiate these effloresced (i.e., darkened) droplets from those that retained their brightness following a SERS scan. The droplets that retain their brightness are aqueous droplets that only partially lost their initial water content. Homogenous pH nanoprobe SERS maps of these aqueous droplets reflect the homogenous distribution of the nanoprobes within the aqueous droplet residue (Figure 1b).

The droplet pH values measured via room-temperature SERS exhibit discrepancies between aqueous droplets and effloresced droplets. The mean droplet pH values of effloresced droplets are 1–2 pH unit higher than the corresponding aqueous droplets (Figure 1c) and exhibit greater variability as denoted by their large standard deviations. This inconsistency in pH shows that the loss of water content, especially if it results in a phase-transition (e.g., efflorescence), impairs the accuracy of pH measurement using room-temperature SERS. Moreover, the measured value may no longer reflect droplet pH as the phase-transition may affect the spectral behavior of the pH nanoprobes. Therefore, to achieve accurate pH characterization for environmental droplets with low solute concentration, it is important to maintain droplet stability.

Using pH paper method on low concentration environmental water samples.

Ault et al. developed a pH paper-based colorimetric method for pH quantification in aerosols and droplets that was recently adapted by Angle et al. to investigate the acidity of sea spray aerosols.[36,37] Herein, we tested this approach to quantify environmental droplet pH. Our results indicate that pH paper exhibits a solute concentration threshold below which it is not possible to achieve accurate pH measurement. As shown in Figure 2a, when the solute concentration was relatively high (>10mM), pH paper accurately measures solution pH; however, when the solute concentration was ~1-3mM, the pH paper exhibited very similar colors over a wide range of solution pH values. This result suggests that use of pH paper may lead to inaccurate results when quantifying the pH of environmental samples with low solute concentrations. To test this hypothesis, we measured pH of bulk environmental samples and their aerosolized samples using pH paper (Figure 2a). For stream water samples, DP and its upstream sample SC, both of which have high salt concentrations, had accurate pH readings (i.e., consistent pH values measured by both pH paper and pH meter) whereas the pH paper results for other samples deviated from those obtained using a pH meter. No pH deviation was observed between the spray samples (i.e., the pH of micron-size droplets) and bulk samples of DP and SC. Since the rain and snowmelt solute concentrations are lower than those for the stream water sample, the results obtained using pH paper are likely inaccurate.

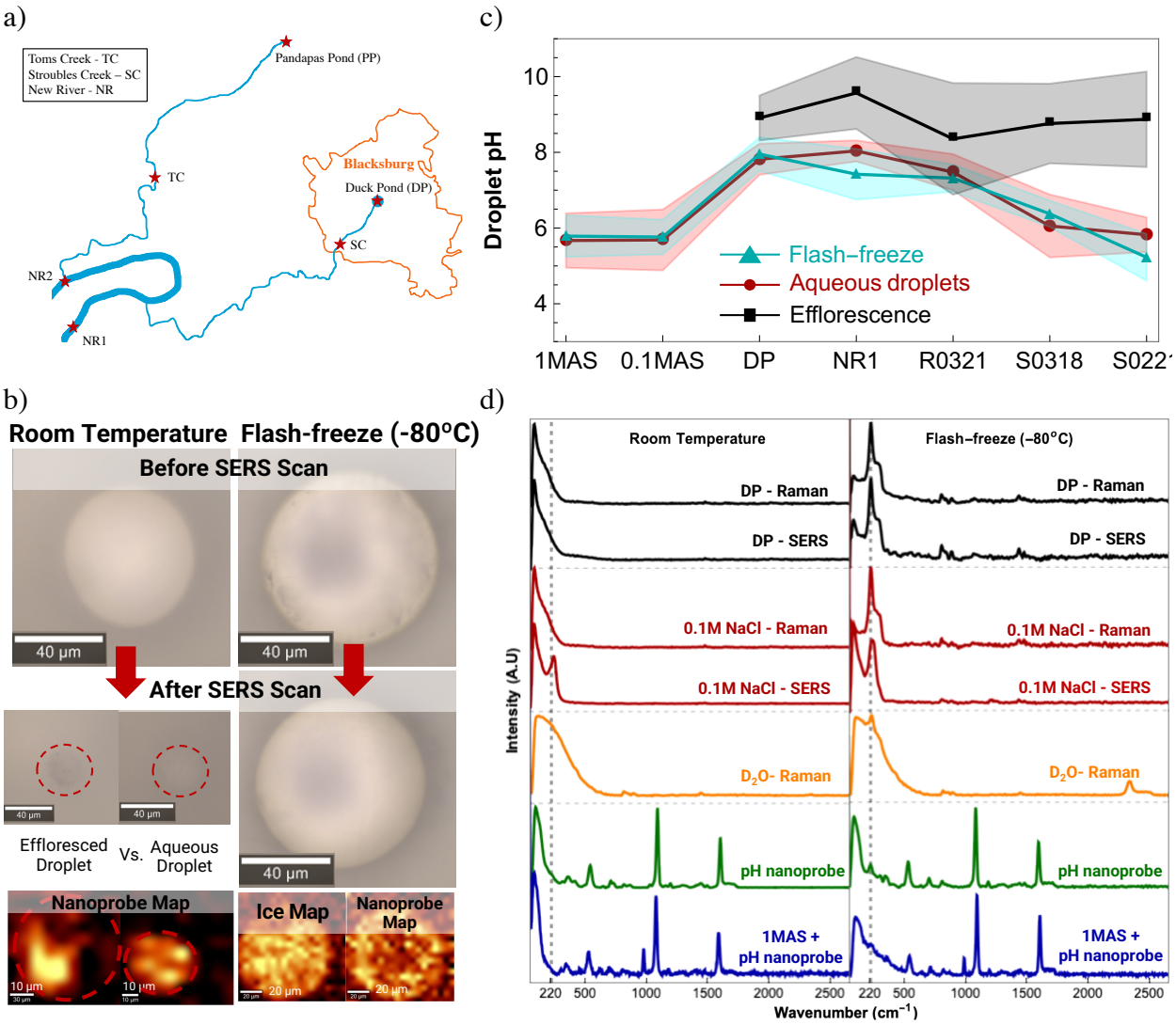

Figure 1. a) Sampling locations and annotations for stream water samples. All rain and snowmelt samples were collected near Blacksburg, Virginia. b) Optical images of collected droplets at room temperature and -80 °C before and after SERS scan. Droplets shrank and evaporated during SERS measurement at room temperature, but remained unchanged during SERS scan at -80 °C. The nanoprobe maps at the bottom were generated based upon the signal intensity of the characteristic peak at 1076 cm^{-1} (reflecting the ring-breathing mode of benzene in 4-MBA). The ice map was generated according to the peak at 220 cm^{-1} that reflects lattice vibration. The SERS maps showed relatively homogeneous distributions of nanoprobe and ice crystals. c) Comparison between room temperature SERS (aqueous), flash-freeze SERS, and measurement results for effloresced-droplets, the shaded area denotes the standard deviation of measurement results. d) Raman and SERS spectra of one environmental water sample (DP – duck pond), 0.1M NaCl, D_2O, pH nanoprobe, and 1M AS + pH nanoprobe at room temperature and at -80 °C in droplets. Except for the spectra of the pH nanoprobe all other SERS spectra were collected from a mixture of the sample and AuNS.

Droplet pH characterization with flash-freeze SERS

Droplets are stable during the flash-freeze SERS measurement, which can be indicated by the consistent size and the brightness of the droplets before and after SERS scanning at -80°C (Figure 1b). In our recent work, we observed a spectral change for the pH nanoprobe in ammonium sulfate (AS) droplets at -50°C which was attributed to aggregation of the pH nanoprobe during ice nucleation and crystal growth that arose due to a moderate temperature decreasing rate (10°C/min).[38] Herein, according to the SERS images, the pH nanoprobes were homogeneously distributed without aggregation at -80°C in flash-frozen droplets. The flash-freeze method suppresses transport and localization of droplet components that can occur under slower temperature changing rates due to nucleation and ice crystal formation.[27,39,40]

The preservation of droplet properties by the flash-freezing process is reflected in the Raman and SERS spectra, as well as SERS images of the droplets. We investigated the change in the Raman and SERS spectra of an environmental water sample (Duck Pond, DP) and a 0.1M NaCl solution between room temperature and -80 °C after flash-freezing (Figure 1d). NaCl is a common solute in environmental water samples and we focus on the spectra of DP due to its high solute concentration (Table S1). The SERS spectra, except for those obtained using pH nanoprobes, were collected from a mixture of synthesized AuNS and a given sample. Upon freezing, strong peaks at ~220cm^{-1} appeared in all sample spectra, but with variations in peak shape. In the Raman spectra of 0.1M NaCl and DP and in the SERS spectra of DP (Figure 1d), the peak at ~220cm^{-1} (with a shoulder at ~280cm^{-1}) appeared only after flash-freezing. This peak corresponds to the literature reported value of the translational lattice vibration of ice[41,42] and therefore reflects ice formation. To test this hypothesis, we collected Raman spectra of D_2O at room temperature and at -80°C. The peak at 220cm^{-1} remained at the same wave number which indicated that the peak arises from

lattice vibrations instead of bond vibrations. The SERS spectra of 0.1M NaCl show negligible change after flash-freezing. Under these conditions, the strong peak at ~220cm^{-1} reflects the combination of the characteristic peak of the Au-Cl covalent interaction and ice.[43] Moreover, no apparent spectral changes were observed in 1M AS droplets (Figure 1d). The SERS and Raman spectra of 0.1M NaCl, DP, and 1M AS suggest that, for a wide range of solute species and concentrations, flash-freeze SERS preserves droplet composition with the phase-transition of water being the major change observed between room-temperature SERS and flash-freeze SERS spectra. The homogeneous SERS image of ice generated according to the intensity of 220cm^{-1} peak from the intermolecular vibration suggests the suppression of solute aggregation, thus resulting in negligible change in sample spectra during the flash-freeze process. The similar Raman spectra (reflecting only ice formation), identical SERS spectra, and homogeneous SERS images collectively demonstrate that the flash-freeze process preserved the properties and the solute component distribution in droplets.

We next investigated the droplet pH values using both room temperature SERS and flash-freeze SERS (Figure 2b). Droplets generated from lab-prepared ammonium sulfate (AS) solutions, stream water samples, rain, and snowmelt samples were investigated. We previously characterized AS droplets and observed both 1M and 0.1M AS droplets are stable during room temperature SERS measurements.[23] Herein, the pH values for AS droplets were consistent between room temperature SERS and flash-freeze SERS and agree with our previously reported values (Figure 1c&1d).[23] This consistent pH measurement result suggests that the flash-freeze process preserves the spectral response of the pH nanoprobe and provides accurate pH measurements. For droplets generated from environmental samples, the pH values measured for aqueous droplet residues via room temperature SERS are similar to those measured for frozen droplets using flash-freeze SERS. The

difference between the mean values of the two methods were insignificant and smaller than 0.5 pH unit; however, aqueous droplet residues were only a small portion of the total droplets with the majority experiencing efflorescence. The confirmation of the aqueous state requires collection of optical images prior to and post SERS measurements. In contrast, the flash-freeze SERS approach enhances the success of a given SERS measurement since it preserves droplet properties. The consistent pH measurement results suggest that in the concentration range involved in this study, the loss of water had a negligible effect on droplet pH. According to Table S1, the total solute concentration in the environmental water samples ranged from ~5-30ppm, which corresponds to ~0.1-1mM. Our optical images of initial droplets and their aqueous residues suggest that an approximate 10× enrichment factor can be applied due to the loss of water content (calculated based upon the change in droplet volume); therefore, the final solute concentration in droplet aqueous residues should be ~50-300ppm, and ~1-10mM. The flash-freeze SERS measured pH for stream water spray droplets was consistent with literature values for sea and lake spray aerosols thus validating the pH value measured by flash-freeze SERS.[3,7]

The bulk sample pH and droplet pH measured using flash-freeze SERS are shown in Figure 2b and representative SERS spectra for pH calculation can be found in Figure S4. No apparent pH difference was observed between bulk stream water and these droplets. For the rain and snowmelt samples, we observed slightly lower pH in snowmelt droplets compared to rain droplets and stream water droplets. We also acidified the collected samples with low concentration H_2SO_4 (1-5mM) to mimic atmospherically relevant aerosol droplets. The droplet pH characterized using flash-freeze SERS was consistent with that measured in the corresponding bulk solutions (Figure 2b). The droplet pH of R0818 exhibited a significantly higher droplet pH compared to the bulk sample pH. We investigated the concentration of ions and the relative ratio between the equivalent major

cations and anions by ICP-MS (Figure 2c). The cation/anion ratio was estimated using $\frac{[Na^+]+[K^+]+2\times([Mg^{2+}]+[Ca^{2+}])}{2\times[SO_4^{2-}]+[Cl^-]}$. The ICP-MS result showed that the cation/anion ratio of the R0818 sample (0.14) was significantly lower than that of other environmental samples (between 1 to 2.8) and the calcium concentration in snowmelt samples was significantly lower than in other samples. The lower calcium concentration explains the lower pH observed in snowmelt droplets. We note that the ICP-MS results do not present all possible compositions that are present in rainwater (e.g., ammonium and carbonate were not measured); however, the difference in the calculated cation/anion ratios reflects the substantial composition difference between the R0818 sample and other environmental water samples. We thus infer the difference in pH between droplets and bulk reflects this composition difference. The ICP-MS result showed that, among characterized species, Na^+, K^+, and SO_4^{2-} are most abundant in the R0818 sample, whereas in other samples Cl^- is comparable or even more dominant (Table S1). We have previously reported that Na_2SO_4 droplets exhibit higher pH values compared to their bulk solution (~1-2 pH unit), potentially due to the preferred solvation of sulfate away from the air-water interface, which is consistent with our observations for R0818.[23]

In addition to determining mean pH values, flash-freeze SERS can also provide 2D pH distributions and component distributions within droplets reflecting all of the collected SERS spectra (Figure S5). Such SERS images can help investigate pH effects near the air-water interface and their relation to component distribution. This is critical for both low concentration and high concentration aerosol droplets in the environment. Moreover, through adjustments to the aerosolization and collection process (e.g., application of flow tube), we can potentially apply flash-freeze SERS on-site to characterize field collected environmental droplets with minimal concern for the effect of the Raman laser on droplet stability.

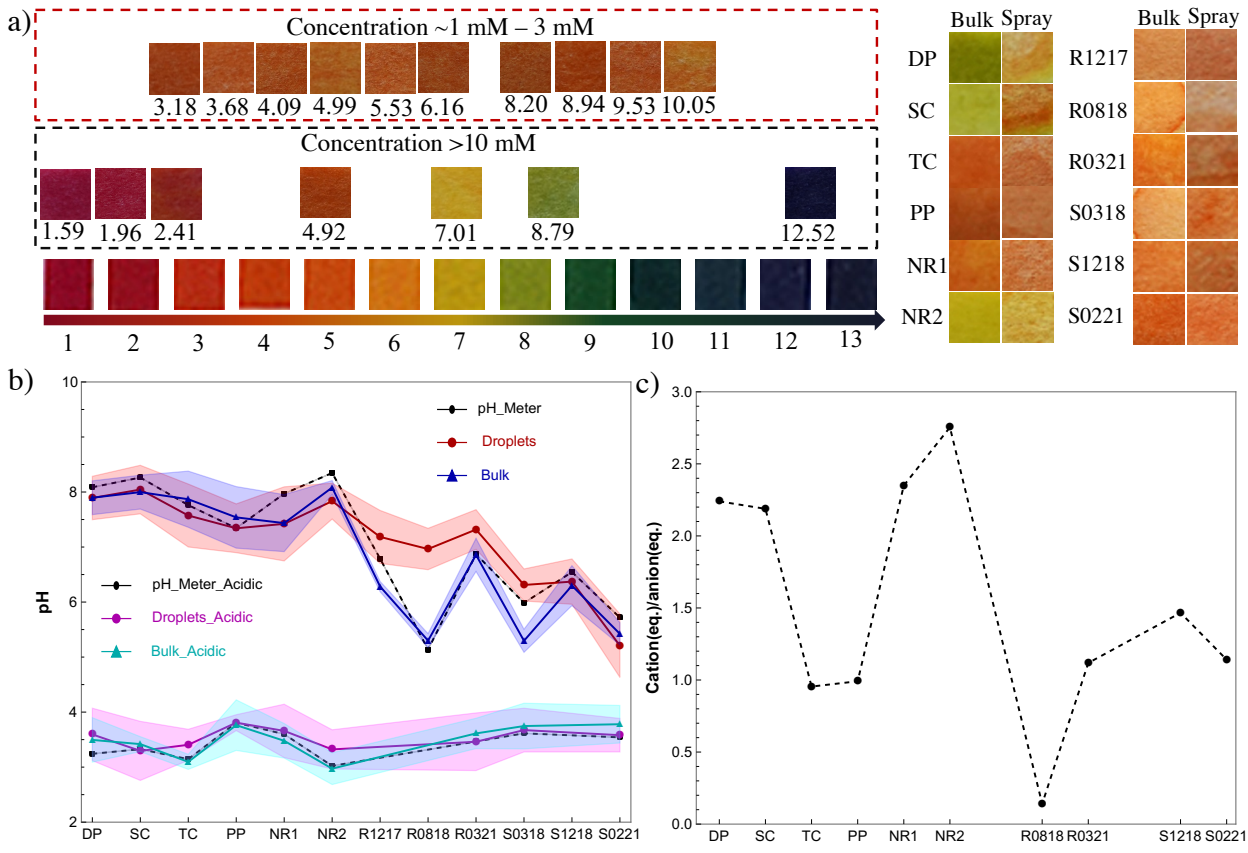

Figure 2. a) The results of pH paper measurements and the effect of solution concentration. For low concentration solutions (1 – 3 mM), the pH paper showed similar color over a wide range of solution pH. b) Measured pH values of environmental samples, and acidic samples made from the environmental samples (pH was adjusted using <10mM H_2SO_4). Bulk pH values of environmental samples were measured by room temperature SERS and the corresponding droplet pH values were measured using flash-freeze SERS. c) The cation/anion ratio of characterized environmental samples according to the ICP-MS result.

Associated Content:

Supporting Information. Synthesis and characterization of pH nanoprobe and AuNS, additional table (Table S1) and graphs (Figure S1-S5) involved in the discussion are included in the supporting information.

Author Information:

Corresponding Author: Peter J. Vikesland – Virginia Tech, Blacksburg, Virginia; Email: pvikes@vt.edu.

Acknowledgment

This research was supported by the National Science Foundation (CBET-1705653). We thank Dr. Weinan Leng for assistance in Reman experiments, and the Virginia Tech Center for Sustainable Nanotechnology for providing the instruments.

References

(1) Zheng, G.; Su, H.; Wang, S.; Andreae, M. O.; Pöschl, U.; Cheng, Y. *Multiphase Buffer Theory Explains Contrasts in Atmospheric Aerosol Acidity*; 2020; Vol. 369. https://doi.org/10.1126/SCIENCE.ABA3719.

(2) Rindelaub, J. D.; Craig, R. L.; Nandy, L.; Bondy, A. L.; Dutcher, C. S.; Shepson, P. B.; Ault, A. P. Direct Measurement of PH in Individual Particles via Raman Microspectroscopy and Variation in Acidity with Relative Humidity. *J. Phys. Chem. A* **2016**, *120* (6), 911–917. https://doi.org/10.1021/acs.jpca.5b12699.

(3) Pye, H.; Nenes, A.; Alexander, B.; Ault, A.; Barth, M.; Clegg, S.; Collett Jr., J.; Fahey, K.; Hennigan, C.; Herrmann, H.; Kanakidou, M.; Kelly, J.; Ku, I.-T.; McNeill, V. F.; Riemer, N.; Schaefer, T.; Shi, G.; Tilgner, A.; Walker, J.; Wang, T.; Weber, R.; Xing, J.; Zaveri, R.; Zuend, A. The Acidity of Atmospheric Particles and Clouds. *Atmos. Chem. Phys.* **2020**, *20* (8), 4809–4888. https://doi.org/10.5194/acp-2019-889.

(4) Freedman, M. A.; Ott, E. J. E.; Marak, K. E. Role of PH in Aerosol Processes and Measurement Challenges. *J. Phys. Chem. A* **2019**, *123* (7), 1275–1284. https://doi.org/10.1021/acs.jpca.8b10676.

(5) Keene, W. C.; Pszenny, A. A. P.; Maben, J. R.; Sander, R. Variation of Marine Aerosol

Acidity with Particle Size. *Geophys. Res. Lett.* **2002**, *29* (7), 5-1-5–4. https://doi.org/10.1029/2001GL013881.

(6) Alexander, B.; Park, R. J.; Jacob, D. J.; Li, Q. B.; Yantosca, R. M.; Savarino, J.; Lee, C. C. W.; Thiemens, M. H. Sulfate Formation in Sea-Salt Aerosols: Constraints from Oxygen Isotopes. *J. Geophys. Res. D Atmos.* **2005**, *110* (10), 1–12. https://doi.org/10.1029/2004JD005659.

(7) Bondy, A. L.; Wang, B.; Laskin, A.; Craig, R. L.; Nhliziyo, M. V.; Bertman, S. B.; Pratt, K. A.; Shepson, P. B.; Ault, A. P. Inland Sea Spray Aerosol Transport and Incomplete Chloride Depletion: Varying Degrees of Reactive Processing Observed during SOAS. *Environ. Sci. Technol.* **2017**, *51* (17), 9533–9542. https://doi.org/10.1021/acs.est.7b02085.

(8) Ault, A. P. Aerosol Acidity: Novel Measurements and Implications for Atmospheric Chemistry. *Acc. Chem. Res.* **2020**, *53* (9), 1703–1714. https://doi.org/10.1021/acs.accounts.0c00303.

(9) Biskos, G.; Malinowski, A.; Russell, L. M.; Buseck, P. R.; Martin, S. T. Nanosize Effect on the Deliquescence and the Efflorescence of Sodium Chloride Particles. *Aerosol Sci. Technol.* **2006**, *40* (2), 97–106. https://doi.org/10.1080/02786820500484396.

(10) McGraw, R.; Lewis, E. R. Deliquescence and Efflorescence of Small Particles. *J. Chem. Phys.* **2009**, *131* (19), 194705. https://doi.org/10.1063/1.3251056.

(11) Köhler, H. The Nucleus in and the Growth of Hygroscopic Droplets. *Trans. Faraday Soc.* **1936**, *32* (0), 1152–1161. https://doi.org/10.1039/TF9363201152.

(12) Wang, N.; Jing, B.; Wang, P.; Wang, Z.; Li, J.; Pang, S.; Zhang, Y.; Ge, M. Hygroscopicity and Compositional Evolution of Atmospheric Aerosols Containing Water-Soluble Carboxylic Acid Salts and Ammonium Sulfate: Influence of Ammonium Depletion. *Environ. Sci. Technol.* **2019**, *53* (11), 6225–6234. https://doi.org/10.1021/acs.est.8b07052.

(13) Peter Larkin. *Infrared and Raman Spectroscopy, 2nd Edition*, 2nd ed.; Elsevier, 2017.

(14) Ault, A. P.; Zhao, D.; Ebben, C. J.; Tauber, M. J.; Geiger, F. M.; Prather, K. A.; Grassian, V. H. Raman Microspectroscopy and Vibrational Sum Frequency Generation Spectroscopy as Probes of the Bulk and Surface Compositions of Size-Resolved Sea Spray Aerosol Particles. *Phys. Chem. Chem. Phys.* **2013**, *15* (17), 6206. https://doi.org/10.1039/c3cp43899f.

(15) Langer, J.; de Aberasturi, D. J.; Aizpurua, J.; Alvarez-Puebla, R. A.; Auguié, B.; Baumberg, J. J.; Bazan, G. C.; Bell, S. E. J.; Boisen, A.; Brolo, A. G.; Choo, J.; Cialla-May, D.; Deckert, V.; Fabris, L.; Faulds, K.; Javier García de Abajo, F.; Goodacre, R.; Graham, D.; Haes, A. J.; Haynes, C. L.; Huck, C.; Itoh, T.; Käll, M.; Kneipp, J.; Kotov, N. A.; Kuang, H.; Le Ru, E. C.; Lee, H. K.; Li, J. F.; Ling, X. Y.; Maier, S. A.; Mayerhöfer, T.; Moskovits, M.; Murakoshi, K.; Nam, J. M.; Nie, S.; Ozaki, Y.; Pastoriza-Santos, I.; Perez-Juste, J.; Popp, J.; Pucci, A.; Reich, S.; Ren, B.; Schatz, G. C.; Shegai, T.; Schlücker, S.; Tay, L. L.; George Thomas, K.; Tian, Z. Q.; van Duyne, R. P.; Vo-Dinh, T.; Wang, Y.; Willets, K. A.; Xu, C.; Xu, H.; Xu, Y.; Yamamoto, Y. S.; Zhao, B.; Liz-Marzán, L. M. Present and Future of Surface-Enhanced Raman Scattering. *ACS Nano* **2020**, *14* (1), 28–117. https://doi.org/10.1021/acsnano.9b04224.

(16) Gong, K.; Jones, R. R.; Li, K.; Xu, G.; Cheng, H.; Feng, Y.; Valev, V. K.; Zhang, L. Sensing

PH of Individual Microdroplet by Combining SERS and Indicator Paper. *Sensors Actuators B Chem*. **2021**, *346*. https://doi.org/10.1016/j.snb.2021.130521.

(17) Yue, S.; Sun, X. T.; Wang, Y.; Zhang, W. S.; Xu, Z. R. Microparticles with Size/Charge Selectivity and PH Response for SERS Monitoring of 6-Thioguanine in Blood Serum. *Sensors Actuators, B Chem*. **2018**, *273*, 1539–1547. https://doi.org/10.1016/j.snb.2018.07.062.

(18) Bi, L.; Wang, Y.; Yang, Y.; Li, Y.; Mo, S.; Zheng, Q.; Chen, L. Highly Sensitive and Reproducible SERS Sensor for Biological PH Detection Based on a Uniform Gold Nanorod Array Platform. *ACS Appl. Mater. Interfaces* **2018**, *10* (18), 15381–15387. https://doi.org/10.1021/acsami.7b19347.

(19) Zou, X.; Wang, Y.; Liu, W.; Chen, L. M -Cresol Purple Functionalized Surface Enhanced Raman Scattering Paper Chips for Highly Sensitive Detection of PH in the Neutral PH Range. *Analyst* **2017**, *142* (13), 2333–2337. https://doi.org/10.1039/c7an00653e.

(20) Ault, A. P.; Axson, J. L. Atmospheric Aerosol Chemistry: Spectroscopic and Microscopic Advances. *Anal. Chem*. **2017**, *89* (1), 430–452. https://doi.org/10.1021/acs.analchem.6b04670.

(21) Wei, H.; Willner, M. R.; Marr, L. C.; Vikesland, P. J. Highly Stable SERS PH Nanoprobes Produced by Co-Solvent Controlled AuNP Aggregation. *Analyst* **2016**, *141* (17), 5159–5169. https://doi.org/10.1039/c6an00650g.

(22) Wei, H.; Vejerano, E. P.; Leng, W.; Huang, Q.; Willner, M. R.; Marr, L. C.; Vikesland, P. J. Aerosol Microdroplets Exhibit a Stable PH Gradient. *Proc. Natl. Acad. Sci*. **2018**, *115*

(28), 7272–7277. https://doi.org/10.1073/pnas.1720488115.

(23) Huang, Q.; Wei, H.; Marr, L. C.; Vikesland, P. J. Direct Quantification of the Effect of Ammonium on Aerosol Droplet PH. *Environ. Sci. Technol.* **2021**, *55* (1), 778–787. https://doi.org/10.1021/acs.est.0c07394.

(24) Brongersma, M. L.; Halas, N. J.; Nordlander, P. Plasmon-Induced Hot Carrier Science and Technology. *Nat. Nanotechnol.* **2015**, *10* (1), 25–34. https://doi.org/10.1038/nnano.2014.311.

(25) Caldarola, M.; Albella, P.; Cortés, E.; Rahmani, M.; Roschuk, T.; Grinblat, G.; Oulton, R. F.; Bragas, A. V.; Maier, S. A. Non-Plasmonic Nanoantennas for Surface Enhanced Spectroscopies with Ultra-Low Heat Conversion. *Nat. Commun.* **2015**, *6*. https://doi.org/10.1038/ncomms8915.

(26) Wei, H.; Loeb, S. K.; Halas, N. J.; Kim, J. H. Plasmon-Enabled Degradation of Organic Micropollutants in Water by Visible-Light Illumination of Janus Gold Nanorods. *Proc. Natl. Acad. Sci. U. S. A.* **2020**, *117* (27), 15473–15481. https://doi.org/10.1073/pnas.2003362117.

(27) Kucinski, T. M.; Ott, E. J. E.; Freedman, M. A. Flash Freeze Flow Tube to Vitrify Aerosol Particles at Fixed Relative Humidity Values. *Anal. Chem.* **2020**, *92* (7), 5207–5213. https://doi.org/10.1021/acs.analchem.9b05757.

(28) Hurbain, I.; Sachse, M. The Future Is Cold: Cryo-Preparation Methods for Transmission Electron Microscopy of Cells. *Biol. Cell* **2011**, *103* (9), 405–420. https://doi.org/10.1042/bc20110015.

(29) Ott, E.-J. E.; Kucinski, T. M.; Dawson, J. N.; Freedman, M. A. Use of Transmission Electron Microscopy for Analysis of Aerosol Particles and Strategies for Imaging Fragile Particles. *Anal. Chem.* **2021**, *93* (33), 11347–11356. https://doi.org/10.1021/acs.analchem.0c05225.

(30) Dubochet, J.; McDowall, A. W. Vitrification of Pure Water for Electron Microscopy. *J. Microsc.* **1981**, *124* (3), 3–4. https://doi.org/10.1111/j.1365-2818.1981.tb02483.x.

(31) Dubochet, J. Cryo-EM-the First Thirty Years. *J. Microsc.* **2012**, *245* (3), 221–224. https://doi.org/10.1111/j.1365-2818.2011.03569.x.

(32) Leng, W.; Vikesland, P. J. MGITC Facilitated Formation of AuNP Multimers. *Langmuir* **2014**, *30* (28), 8342–8349. https://doi.org/10.1021/la501807n.

(33) Yuan, H.; Khoury, C. G.; Hwang, H.; Wilson, C. M.; Grant, G. A.; Vo-Dinh, T. Gold Nanostars: Surfactant-Free Synthesis, 3D Modelling, and Two-Photon Photoluminescence Imaging. *Nanotechnology* **2012**, *23* (7). https://doi.org/10.1088/0957-4484/23/7/075102.

(34) Braun, C.; Krieger, U. K. Two-Dimensional Angular Light-Scattering in Aqueous NaCl Single Aerosol Particles during Deliquescence and Efflorescence. *Opt. Express* **2001**, *8* (6), 314. https://doi.org/10.1364/oe.8.000314.

(35) Lundgren, D. A.; Cooper, D. W. Effect of Humidify on Light-Scattering Methods of Measuring Particle Concentration. *J. Air Pollut. Control Assoc.* **1969**, *19* (4), 243–247. https://doi.org/10.1080/00022470.1969.10466482.

(36) Craig, R. L.; Peterson, P. K.; Nandy, L.; Lei, Z.; Hossain, M. A.; Camarena, S.; Dodson, R.

A.; Cook, R. D.; Dutcher, C. S.; Ault, A. P. Direct Determination of Aerosol PH: Size-Resolved Measurements of Submicrometer and Supermicrometer Aqueous Particles. *Anal. Chem.* **2018**, *90* (19), 11232–11239. https://doi.org/10.1021/acs.analchem.8b00586.

(37) Angle, K. J.; Crocker, D. R.; Simpson, R. M. C.; Mayer, K. J.; Garofalo, L. A.; Moore, A. N.; Mora Garcia, S. L.; Or, V. W.; Srinivasan, S.; Farhan, M.; Sauer, J. S.; Lee, C.; Pothier, M. A.; Farmer, D. K.; Martz, T. R.; Bertram, T. H.; Cappa, C. D.; Prather, K. A.; Grassian, V. H. Acidity across the Interface from the Ocean Surface to Sea Spray Aerosol. *Proc. Natl. Acad. Sci. U. S. A.* **2021**, *118* (2). https://doi.org/10.1073/pnas.2018397118.

(38) Huang, Q.; Vikesland, P. J. Low-Temperature Raman Imaging of Component Distribution in Micron-Size Droplets. *ACS Earth Sp. Chem.* **2022**, *6* (1), 239–248. https://doi.org/10.1021/acsearthspacechem.1c00412.

(39) Bogdan, A. Double Freezing of (NH4)2SO4/H 2O Droplets below the Eutectic Point and the Crystallization of (NH4)2SO4 to the Ferroelectric Phase. *J. Phys. Chem. A* **2010**, *114* (37), 10135–10139. https://doi.org/10.1021/jp105699s.

(40) Chong, E.; King, M.; Marak, K. E.; Freedman, M. A. The Effect of Crystallinity and Crystal Structure on the Immersion Freezing of Alumina. *J. Phys. Chem. A* **2019**, *123* (12), 2447–2456. https://doi.org/10.1021/acs.jpca.8b12258.

(41) Johari, G. P.; Chew, H. A. M.; Sivakumar, T. C. Effect of Temperature and Pressure on Translational Lattice Vibrations and Permittivity of Ice. *J. Chem. Phys.* **1984**, *80* (10), 5163–5169. https://doi.org/10.1063/1.446587.

(42) Fukazawa, H.; Mae, S.; Ikeda, S.; Watanabe, O. Proton Ordering in Antarctic Ice Observed

by Raman and Neutron Scattering. *Chem. Phys. Lett.* **1998**, *294* (6), 554–558. https://doi.org/10.1016/S0009-2614(98)00908-7.

(43) Chan, M. Y.; Leng, W.; Vikesland, P. J. Surface-Enhanced Raman Spectroscopy Characterization of Salt-Induced Aggregation of Gold Nanoparticles. *ChemPhysChem* **2018**, *19* (1), 24–28. https://doi.org/10.1002/cphc.201700798.